Nuclear Instruments and Methods in Physics Research A 1058 (2024) 168856

Contents lists available at ScienceDirect

Nuclear Inst. and Methods in Physics Research, A

journal homepage: www.elsevier.com/locate/nima

Full Length Article

A versatile wide energy range spectrometer for soft X-ray FELs

Emiliano Principi [a,*], Cristian Svetina [b,c,*], Dario De Angelis [d], Claudio Fava [a], Riccardo Mincigrucci [a], Laura Foglia [a], Alberto Simoncig [a], Michele Manfredda [a], Nicola Mahne [a,d], Riccardo Gobessi [a], Martin Scarcia [a], Alessandro Gessini [a], Filippo Bencivenga [a], Flavio Capotondi [a], Marco Zangrando [a,d], Claudio Masciovecchio [a]

[a] Elettra-Sincrotrone Trieste S.C.p.A., Strada Statale 14 - km 163.5, 34149 Basovizza, Trieste, Italy
[b] Instituto Madrileño de Estudios Avanzados en Nanociencia, C/ Faraday 9, 28049, Madrid, Spain
[c] European XFEL, Holzkoppel 4, 22869, Schenefeld, Germany
[d] CNR-IOM, Strada Statale 14 - km 163.5, 34149 Basovizza, Trieste, Italy

ARTICLE INFO

Keywords:
Free electron lasers
Soft X-ray spectrometer
Single-shot measurements
Ultrafast experiments
Transmission geometry
Ray tracing

ABSTRACT

The design and main characteristics of the Wide Energy range Spectrometer at TIMEX (WEST) operating at the FERMI Free Electron Laser are described. WEST covers the entire photon energy range of the FERMI source including its fundamental emission (extreme ultraviolet region, EUV) and its highest harmonics (soft X-ray region) spanning about a thousand of electrovolts from 20 to 1000 eV. The instrument is specifically designed to measure FERMI FEL spectra with good resolving power ($500 < RP < 7000$) and provide remarkable signal to noise ratio adequate for single-shot experiments. Notably, WEST is aligned in transmission geometry downstream of the TIMEX experimental beamline thus offering a valid diagnostic tool for the characterization of both linear and nonlinear spectral effects driven by the interaction between FEL radiation and samples in gaseous, liquid and solid phase. Detailed theoretical analysis of the instrument performance complemented by experimental measurements is presented. Further possible upgrades of WEST are finally considered and discussed.

1. Introduction

The characterization and operation of X-ray Free Electron Lasers (FELs) sources require continuous monitoring of the spectral properties of the emitted light pulses. As a consequence, X-ray FEL facilities are equipped with dedicated extreme ultraviolet (EUV) or X-ray spectrometers designed to provide FEL spectra with suitable repetition rate, resolution, sensitivity and reliability [1–13]. Spectrometers specialized in analyzing X-ray FEL sources emission are conceived to be almost transparent to the FEL beam thus minimizing the perturbation of the FEL pulses and allowing most of the beam to be at scientists disposal for experiments. In experimental endstations of X-ray FELs, other classes of X-ray spectrometers are typically positioned around the sample environment for investigating the sample response to FEL exposure using photon-in photon-out techniques. Spectrometers for X-ray elastic scattering (e.g. Thomson [14,15]) and resonant inelastic X-ray scattering (RIXS [16–18]) for instance, work in reflection geometry at variable angles to the sample thus scanning various momentum transfers [19–22]. Similarly, X-ray emission spectrometers can be strategically positioned close to the sample and normally to the FEL beam to detect fluorescence lines [23].

Notably, spectrometers placed downstream of the sample, specifically designed for operating on the direct FEL beam in transmission geometry, are less common although this configuration can be extremely important, and sometimes essential, for diverse classes of X-ray FEL experiments. It is worth mentioning those experiments aimed at generating amplified spontaneous emission downstream of a gas sample excited by a X-ray FEL pulse [24]. Other emerging scientific cases that benefit from X-ray spectroscopies in transmission geometry are those involving nonlinear effects on matter driven by intense EUV or soft X-ray FEL pulses. Second harmonic generation (SHG) is a well-known nonlinear process, often used in the visible range, that has been recently observed also in the EUV and X-ray photon energy range [25,26]. SHG can be revealed, for example, by monitoring the spectral lines of high energy photons downstream of ultrathin samples [27,28]. Further nonlinear effects which alter the shape of the FEL spectrum following the interaction of the EUV FEL pulse with submicrometer metallic foils have been observed [29], originated by nonlinear phenomena such as self-phase modulation, still unexplored in the EUV photon energy range.

* Corresponding authors.
E-mail addresses: emiliano.principi@elettra.eu (E. Principi), cristian.svetina@imdea.org (C. Svetina).

https://doi.org/10.1016/j.nima.2023.168856
Received 17 July 2023; Received in revised form 13 October 2023; Accepted 1 November 2023
Available online 3 November 2023

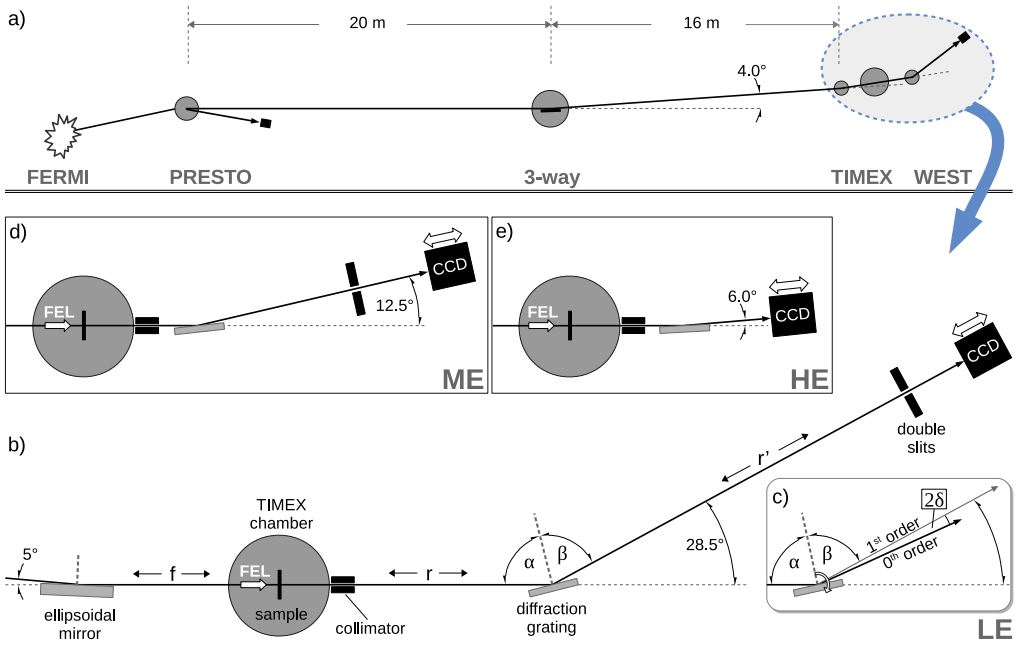

Fig. 1. Sketch of the FERMI FEL beam transport towards TIMEX and configurations of WEST. (a) Position of the spectrometers WEST and PRESTO on the beam transport. (b) Low photon energy (LE) geometry. (c) Angular relationship between the 0th and 1st diffraction order: the deviation angle $2\theta = \alpha + \beta$ is invariant to the FEL wavelength, while the scan angle $2\delta = \alpha - \beta$ between 0th and 1st diffraction order increases with the FEL wavelength. The pitch angle of the grating corresponds to the angle δ. (d) Medium photon energy (ME) configuration. (e) High photon energy (HE) configuration.

Furthermore, transmission geometry X-ray spectrometers can be fruitfully employed for time-resolved X-ray Absorption Spectroscopy (tr-XAS) with FELs. The spectrum of broadband SASE FELs can be measured downstream of the sample thus collecting spectral profiles with single shot exposure [30–32]. A similar geometry can be used also with seeded FELs that deliver very narrow bandwidth pulses whose photon energy can be tuned across selected absorption edges [33,34]. Having a X-ray spectrometer at disposal permits measuring the intensity of the desired wavelength, getting rid of the undesired harmonic content of the seeded FEL source thus improving the quality of the XAS measurements.

Progress with innovative FEL-based transmission spectroscopies has led to promising experimental approaches like the stochastic spectroscopy [35,36] based on the correlation of broadband SASE FEL spectra recorded upstream and downstream of submicrometre samples (typically self standing foils, or thin depositions onto transparent membranes such as Si_3N_4). This technique allows simultaneous collection of both XAS and X-ray emission spectra (XES) operating in transmission geometry. Another FEL emerging method is combining tr-XAS with impulsive stimulated Raman scattering (ISRS) for studying low frequency vibrational modes of complex molecules in the time domain with atomic and enantiomeric selectivity [37]. This approach requires monitoring the ISRS-driven intensity time modulation of the monochromatic narrowband FEL beam downstream of the sample across selected atomic absorption edges. Finally, the development of four-wave mixing methodologies such as Coherent Anti-Stokes Raman Scattering (CARS), is based on spectral analysis of the signal on a shot to shot basis, often in transmission [38].

In this article, the concept, design and commissioning results of the Wide Energy range Spectrometer at TIMEX (WEST) are described. WEST is optimized for single-shot real time monitoring of the spectrum of the FERMI seeded FEL (Trieste, Italy [39–41]) in transmission geometry downstream of gaseous, liquid and solid samples in the TIMEX beamline [42]. Theoretical calculations of relevant parameters of WEST as well as results of ray-tracing simulations are presented. The performance of WEST is put to the test by comparison between single-shot spectra measured by both WEST and the high resolution FERMI's spectrometer PRESTO [6] (Fig. 1a).

2. Technical design

2.1. Overview

The aim of WEST is to provide a compact and cost-effective wide photon energy range spectrometer capable of covering the entire nominal spectral range of the FERMI FEL source including fundamental and highest harmonics (about 20–900 eV, 1.4–60 nm) in compliance with both the stringent limitations of free space around the TIMEX endstation and constraints of the FEL beam transport. Importantly, FERMI is a seeded FEL as the emitted radiation pulse is triggered by the interaction of an ultraviolet fs-laser pulse (also called *seed*) with the relativistic electron bunch [39]. As a result of the seeding process, the FEL pulse inherits some important properties of the seed, including the spectral profile, leading to near Fourier-transform limited EUV pulses. Typical relative spectral bandwidth of FERMI fundamental pulses can be better than 10^{-3}. The optical design of WEST maximizes both efficiency and spectral resolution suitable for monitoring this kind of narrowband FEL emission.

WEST consists of a diffraction grating manufactured by Helmholtz Zentrum Berlin (HZB) and a soft X-ray Charged Coupled Device (CCD) camera by Andor Oxford Instruments normal to the incident beam, positioned on a manual longitudinal translator that allows adjusting the CCD-grating distance (Fig. 1). The grating substrate is a super-polished spherical silicon mirror, already available before defining the grating parameters (Table 1). WEST is conceived as a slitless spectrometer whose source is the FEL micrometric focal spot generated in the vicinity of the experimental samples by an ellipsoidal mirror upstream of the TIMEX chamber [42]. The few micron FEL spot is ideal to maximize both the resolving power of the spectrometer and photon flux at the grating thus enabling the adopted scheme. Moreover, the absence of an entrance slit can be strategic in high fluence experiments that likely cause radiation damage of the slit. In the next subsections, the optimization process, parameters and performances of WEST are described in detail.

Table 1
Diffraction grating main parameters.

Substrate	
Material	Si100
Dimensions	100 × 25 × 15 mm^2
Optical Surface	spherical
Clear aperture	90 × 20 mm^2
Radius of curvature	9.75 m
Tangential slope error (rms)	<0.4 arcsec
Sagittal slope error (rms)	<2 arcsec
Microroughness (rms)	<3 mm
Ruled grating	
Coating material	Au
Coating thickness	32 +/− 4 nm
Groove density	999.98 +/− 0.02 l/mm
Groove depth	11.4 +/− 0.13 nm
Groove width/spacing ratio	0.7 +/− 0.02
Trapezoidal angle	7.5 +/− 0.7 degrees
Micro roughness (rms)	0.3 +/− 0.7 nm

2.2. Geometry

Specific theoretical simulations were carried out to refine the design of WEST. Tuning of the spectrometer parameters at the grating's focus can be done by fulfilling the Fermat condition, minimizing the optical path function by calculating the partial derivatives along the tangential and sagittal directions of the grating [43]. This leads to the well known formulas:

$$k\lambda a = sin(\alpha) - sin(\beta) \tag{1}$$

$$\frac{cos^2(\alpha)}{r} + \frac{cos^2(\beta)}{r'} - \frac{cos(\alpha)+cos(\beta)}{R} = 0 \tag{2}$$

$$\frac{sin(\alpha)}{r}\left(\frac{cos^2(\alpha)}{r} - \frac{cos(\alpha)}{R}\right) - \frac{sin(\beta)}{r'}\left(\frac{cos^2(\beta)}{r'} - \frac{cos(\beta)}{R}\right) = 0 \tag{3}$$

where λ is the photon wavelength, k is the order of diffraction, c the speed of light, r is the entrance arm, r' the exit arm, α and β the incidence and diffraction angle, a the groove density and R the radius of curvature of the substrate.

The energy resolution is then calculated by adding in quadrature three different contributions, namely the source size (ΔE_S), slope errors of the grating (ΔE_{Gr}) and detector pixel size (ΔE_D) [20,44]:

$$\Delta E_S = \frac{E^2 cos(\alpha)}{hck\alpha}\left(\frac{2.64\,\sigma_s}{r}\right) \tag{4}$$

$$\Delta E_{Gr} = \frac{E^2 cos(\alpha)+cos(\beta)}{hck\alpha}\left(2.64\,\sigma_{Gr}\right) \tag{5}$$

$$\Delta E_D = \frac{E^2 cos(\beta)}{hck\alpha}\left(\frac{2.64\,\sigma_D}{r'}\right) \tag{6}$$

$$\Delta E = \sqrt{\Delta E_S^2 + \Delta E_{Gr}^2 + \Delta E_S^2} \tag{7}$$

where E is the photon energy, h the Planck constant ($E(\mathrm{eV}) = hc/\lambda \simeq 1239.842/\lambda(\mathrm{nm})$), σ_S the variance of the source distribution (i.e. the standard deviation of the Gaussian beam), σ_{Gr} rms slope error of the grating and σ_D the variance of the detector spatial resolution (Gaussian-like response). For our study the WEST source nominal size is considered either 2.4 μm or 1.1 μm (rms) depending on the demagnification of the FEL source provided by the ellipsoidal mirror for different undulator chains of the FERMI source, namely FEL1 [39] or FEL2 [40]. The detector pixel size is 13.0 μm and the measured slope error of the substrate is below 1.9 μrad (rms). The overall geometry has been optimized by balancing energy resolution and efficiency using an already available diffraction grating substrate (Table 1). In detail, the best energy resolution was assessed by scanning the deviation ($2\theta = \alpha+\beta$) and scan angles ($2\delta = \alpha-\beta$) (Fig. 1b,c) as well as the entrance/exit arms, the latter varied within the available boundaries (500 mm < r < 2500 mm, r' < 3000 mm). With this approach, three different regimes have been determined, termed low (LE), medium (ME) and high photon energy (HE) range, each of them with its own invariant deviation angle and entrance arm (Fig. 1b,d,e, Table 2). The variable exit arm length has to be adjusted for accommodating the CCD on the grating focal plane as a function of the photon energy. This simplifies the instrument construction and provides a convenient way to move and align the diffraction grating in a compact vacuum chamber.

Table 2
WEST spectrometer main parameters.

Nominal total photon energy range	30–920 eV (1.3–41 nm)
Extended total photon energy range	20–1000 eV (1.24–62 nm)
Nominal photon energy range (LE)	30–159 eV (7.8–41 nm)
Nominal photon energy range (ME)	74–364 eV (3.4–16.8 nm)
Nominal photon energy range (HE)	270–920 eV (1.3–4.6 nm)
f, focal length of the ellipsoidal mirror	1400 mm
r, TIMEX chamber-grating distance (LE)	1900 mm
r, TIMEX chamber-grating distance (ME, HE)	800 mm
r', grating to CCD distance (LE)	2890–3050 mm
r', grating to CCD distance (ME)	1320–1620 mm
r', grating to CCD distance (HE)	480–850 mm
$\alpha+\beta$, deviation angle (LE)	151.5 deg
$\alpha+\beta$, deviation angle (ME)	167.5 deg
$\alpha+\beta$, deviation angle (HE)	174.0 deg

2.3. Efficiency

The fundamental beam of FERMI lies in the extreme ultraviolet region (EUV, 20–300 eV, 4–62 nm) with pulse intensities ranging from a few to hundreds of microJoules. This high level of intensity allows maximizing the spectral resolution of WEST, partially relaxing the requirements for the grating efficiency. The high harmonics emission extends the range of FERMI to the soft X-ray region (300–900 eV, 1.4–4 nm) with a significant attenuation of the pulse intensity, at least 2 orders of magnitude less than the fundamental one [45]. In order to compensate for the reduced FEL source brilliance, WEST is designed for a lower spectral resolution in the soft X-ray, thus gaining more grating efficiency.

A laminar grating profile was preferred to the blazed one as more suitable to operate within the entire broad energy range fulfilling the tight geometrical boundaries. Efficiency simulations carried out with a Neviere's based code (REFLEC [46,47]) over a set of different grating parameters (groove depth, ratio, trapezoidal angle, coating type) has lead to the values shown in Table 1. This solution guarantees efficiencies greater than 3% within almost the whole nominal spectral range of WEST, reaching the maximum values of 22% (LE), 17% (ME) and 12% (HE) (Fig. 2) in the first diffraction order. In the soft X-rays close to 1000 eV where the efficiency dramatically drops, the efficiency of the second diffraction order actually reaches a remarkable value of about 3.5% to be considered when future upgrades of FERMI will further extend the soft X-ray range.

2.4. Ray-tracing simulations and resolving power

Ray tracing simulations were run to validate the results obtained with the theoretical calculations and to check the effect of misalignments and mirror shape errors. The ShadowOUI [48] ray tracing code was used to simulate the FERMI FEL sources, the photon beam transport of TIMEX and finally the WEST spectrometer. In the simulation, the actual profiles of the mirrors composing the beamline were taken into account. The effect of the finite grating longitudinal size (90 mm) and CCD sensor dimension (13.3 mm) was investigated in terms of overall geometrical transmission. The focal distance r' as a function of the FEL wavelength (Fig. 3) and the footprint size of the FEL beam on the grating (Fig. 1S, supplementary material) were calculated for the diverse WEST configurations. Results reveal that the grating intercepts a major fraction of the FEL beam in the spectral region with efficiency greater than 3%.

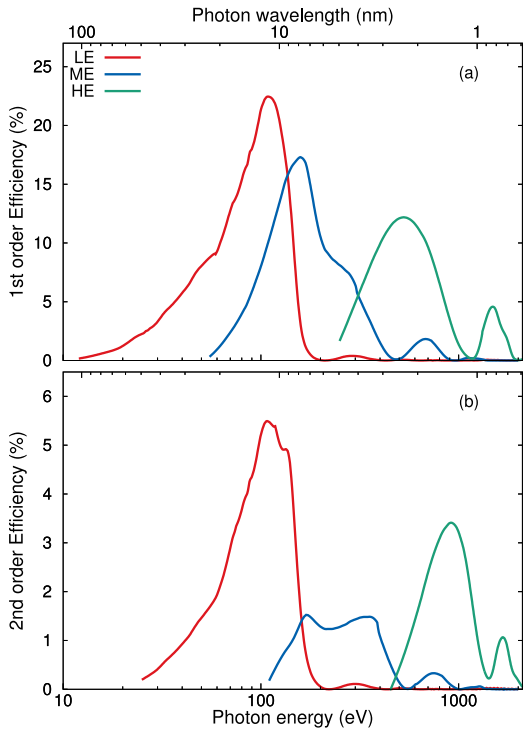

Fig. 2. Theoretical efficiency of the WEST diffraction grating; low (LE), middle (ME) and high photon energy (HE) configurations are represented respectively by red, blue and green curves. (a) first, (b) second diffraction order.

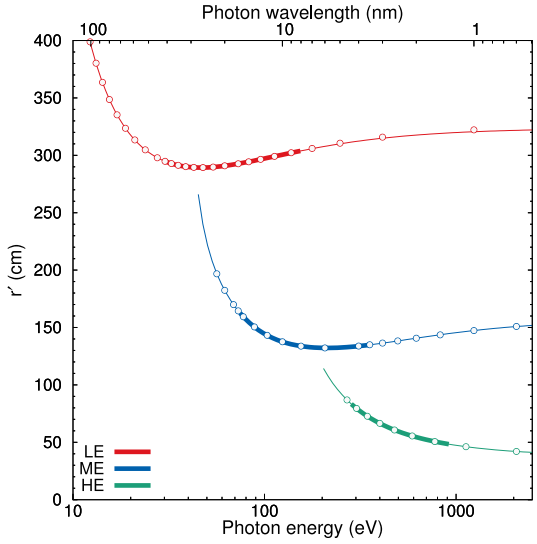

Fig. 3. Distance r' between the diffraction grating and the CCD (Fig. 1, Table 2) for the three configurations of WEST. Empty circles are theoretical calculations, curves are best fit polynomial functions (coefficients in the supplementary material). Thick curves highlight the spectral regions where the diffraction grating exhibits efficiency greater than 3%.

At the longest wavelengths attainable by the WEST configurations, in particular for the LE and ME schemes, the decrease of diffraction efficiency is accompanied by a significant geometrical loss as the FEL beam becomes larger than the size of the grating as an effect of the increasing beam divergence. Moreover, in the LE geometry, this effect is further enhanced by the vertical size of the spectral line that exceeds the dimensions of the CCD sensor. These effects lead to the decrease of the transmitted intensity (supplementary material, Fig1S). Although this is not generally a critical issue, as the FERMI source is very

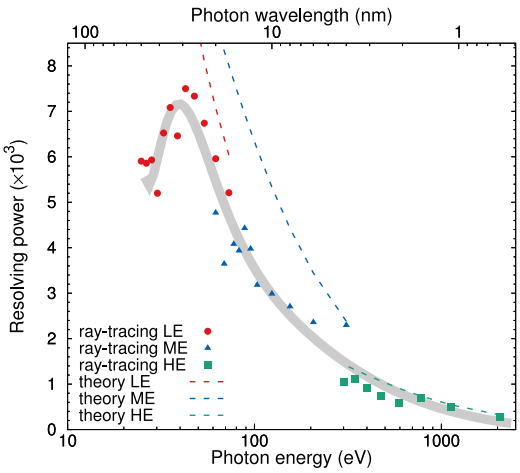

Fig. 4. Resolving power of WEST (first diffraction order, CCD in normal incidence). Filled points are ray-tracing calculations including shape errors of beam transport optics, the thick gray curve is the best fit polynomial function (coefficients in the supplementary material) of ray tracing data. Dashed curves are analytical calculations (Eqs. (1)–(3)).

bright at long wavelengths, it could represent a limitation for certain spectroscopies requiring a pronounced similarity between WEST and PRESTO spectra [36]. Indeed, if the spectral content of the off-axis radiation differs from that of the on-axis mode, WEST and PRESTO could detect different spectra, being separated by a 37 m long beam transport section (Fig. 1a) including various finite size optics [49].

At the shortest wavelengths, in particular for the ME and HE geometries, there is a drastic reduction of the FEL beam footprint (a few mm) associated with the natural contraction of the FEL beam transverse size. This is generally undesired, as the major part of the grating is not illuminated and cannot contribute to the spectral dispersion. The issue can be mitigated by increasing the incidence angle on the grating, however this approach can be in conflict with the geometrical constraints. Therefore, the selected deviation angles of WEST represent a compromise that balances diverse parameters. Ray tracing simulations with realistic mirrors/grating profiles provide a useful estimation of the grating focal length r' as a function of the FEL wavelength (Fig. 3). This information can be helpful for WEST's users to focus the spectral image on the CCD surface by manually adjusting the CCD translation stage position.

Finally, the resolving power ($RP = E/\Delta E$) has been assessed through ray tracing by invoking the Rayleigh criterion for two energy lines (supplementary material, Fig. 2S). The RP parameter reaches the maximum values of about 7000, 4000 and 1000 for the low, medium and high photon energy range, respectively (Fig. 4). The RP obtained by ray tracing is in good agreement with the analytical calculations (Eq. (4)–(7)) in the HE energy range. At longer wavelengths, probed with ME and LE geometries, the ray tracing RP is smaller than the theoretical one. This effect resides in the slope errors of the FERMI beam transport optics, considered in the ray tracing calculations, that get worse towards the edge of the optics thus being more evident for more divergent beams.

The resolving power of WEST can be improved by positioning the CCD detector non-normally to the incoming radiation. Indeed, by rotating the CCD to the right [21,50], the sensor surface gets more aligned with the focal plane of the grating that forms angles of about 17, 8 and 4 degrees with the FEL beam (LE, ME and HE, respectively). Additionally, the effective CCD horizontal pixel size gets compressed when the CCD is tilted. With this approach it would be possible to increase the resolving power of 20%–40% (LE), 30%–70% (ME) and 30%–40% (HE). This geometry can be obtained modifying the Conflat

flange adapter (CF100 to CF40) in front of the CCD's chip (supplementary material). Clearly, operating the CCD in a tilted fashion adversely affects its quantum efficiency and the overall photon sensitivity. A theoretical estimation of the quantum efficiency for normal and almost grazing incidence (70 degrees) for the CCD sensor type "BN" is shown in the supplementary material (Fig. 10S). However, CCD rotations greater than 45 degrees are not allowed as they cause mechanical incompatibility between the Conflat adapter and the camera body. An alternative approach to ameliorate the RP value is to position a pinhole between the experimental sample and the grating. The pinhole limits the beam to the central region of the diffraction grating mitigating the detrimental effects of the slope errors. Therefore, the efficacy of this method is expected to significantly increase with the FEL wavelength. For example, an aperture of diameter 2.5 mm, placed 200 mm upstream of the grating can effectively improve the resolving power of WEST from 6000 up to 13000 at 25 eV (50 nm). Under those conditions, the geometrical transmission is reduced from 55% to 16%.

2.5. Technical implementation

WEST operates in the FEL horizontal plane at a height of 1200 mm from the floor. The entire WEST setup is kept under high vacuum (10^{-7} mbar) by a turbo pump and is connected to the rear gate valve of the TIMEX experimental chamber. The diffraction grating, positioned at a distance r from the TIMEX center where the FEL beam is focused, both spectrally disperses and focuses the FEL beam at a distance r' from the grating (Fig. 1b). The final parameters of both the substrate and grating are listed in Table 2. The grating is positioned in a dedicated high vacuum chamber directly connected with the TIMEX chamber through a DN40 CF straight connector.

The grating can be finely aligned by three independent piezoelectric vacuum motors (SmarAct GmbH) associated with the conventional rotational degrees of freedom (pitch, roll and yaw) and by three linear axes of a manual manipulator. The motorized axes serve to precisely steer the dispersed beam on the CCD. In particular, the rotation of the pitch motor (around the vertical axes of the grating), measured by the angle δ (Fig. 1c), can be adjusted to centering the desired spectral line on the CCD. The manual axes serve to center the grating on the primary FEL beam. The latter is a sporadic operation, usually carried out only prior to starting the experiment. Having an invariant deviation angle for a given photon energy range, the setup requires only one additional manual translation stage that put the CCD in the best focus position defined by r' (Fig. 1).

The used CCD is an Andor iKon-M SO X-ray model [51] equipped with an uncoated back-illuminated 1024 × 1024 sensor (13 μm pixel size). The CCD sensor is optimized for the operation in the EUV and soft X-ray range through an enhanced fabrication process (termed "BEN" [51]) of its surface that substantially improves the quantum efficiency. Moreover, the CCD can be cooled by a Peltier cell that can reach, in combination with a chiller, the temperature of −90 °C. The CCD is integrated with the acquisition system of FERMI and can communicate with it at the repetition rate of the FERMI source (50 Hz) when operated in full vertical binning mode. The CCD readout in imaging mode is possible for a reduced repetition rate (10 Hz), either limiting the image to a small region of interest of the CCD (about 100 rows, possibly on the top half of the CCD) or using a vertical binning of 8 pixels. Full frame images are attainable only for single shot measurements. The Andor camera's body is connected to the grating chamber through a DN40 CF straight connector and an edge welded bellows with a maximum extension of 300 mm. This bellows permits to position the CCD at the desired distance r' from the grating.

Undesired off axis FEL radiation and scattered visible light (seed laser, pump laser or ambient illumination) that can affect the background of the spectrum are mitigated by a cylindrical aluminum collimator with an aperture diameter of 6 mm and length 110 mm positioned between the TIMEX chamber and the diffraction grating (Fig. 1b,d,e). A filter revolver equipped with 7 different metallic thin foils is placed just in front of the collimator in the TIMEX chamber to attenuate the FEL intensity when the CCD is saturated or to further screen visible and infrared scattered light. A set of double slits (both vertical and horizontal) are available in the LE and ME configurations (Fig. 1b,d) for improving screening of residual background light or protecting the CCD from very intense spectral features that adversely affect the measurements.

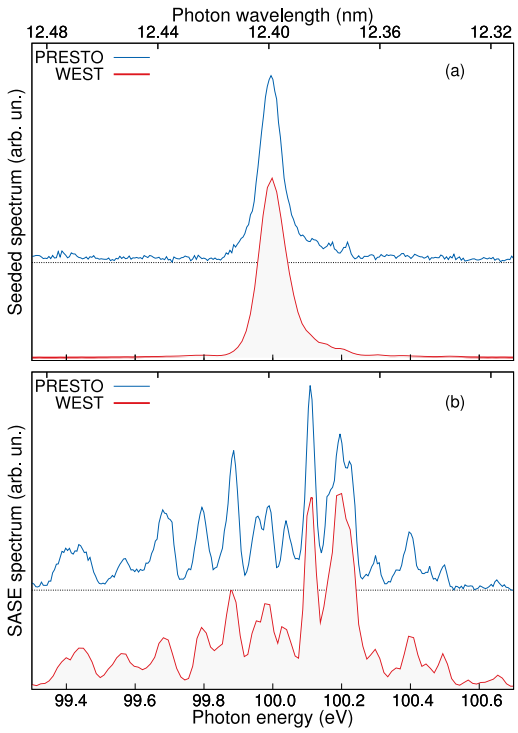

Fig. 5. The WEST spectrometer is compared with the PRESTO spectrometer positioned upstream of the sample, closer to the FERMI FEL source. The PRESTO spectra are vertically shifted for better readability. (a) Example of single shot spectra during seeded FEL operation; (b) example of single shot spectra during SASE FEL operation.

3. Experimental results

The WEST spectrometer was successfully used during various experimental campaigns carried out at the TIMEX beamline. Typical single shot spectra delivered by FERMI at the photon energy of 100 eV in standard seeding mode [29] and SASE optical klystron mode [36] are shown in Fig. 5 as measured by both WEST and PRESTO spectrometers. At 100 eV, the expected resolving power of WEST is about 3500, while that one of PRESTO is about 20000 (using the grating " G2" [6]). The spectra are nicely comparable and very well correlated. This is a really important achievement as the distance between the two spectrometers is considerable (more than 37 m) and WEST was designed with much tighter boundaries than PRESTO and with a single laminar grating only instead of three VLS gratings as for PRESTO.

High shot-to-shot spectral correlation between different measurements of the same FEL spectrum is a crucial prerequisite for various experimental techniques based on the spectral analysis of the FEL beam upstream and downstream of the sample. Pronounced correlation between spectra allows detecting linear and more subtle nonlinear spectral effects driven by the interaction of the intense single FEL pulse with the sample. Typical linear correlation coefficients between integrated spectra intensities of PRESTO and WEST can be larger than 0.99. The second order spectral correlation function ($g^{(2)}$) of PRESTO and WEST spectra across 100 eV reveals that excellent correlation between the two spectrometers can be achieved on a single shot basis [36].

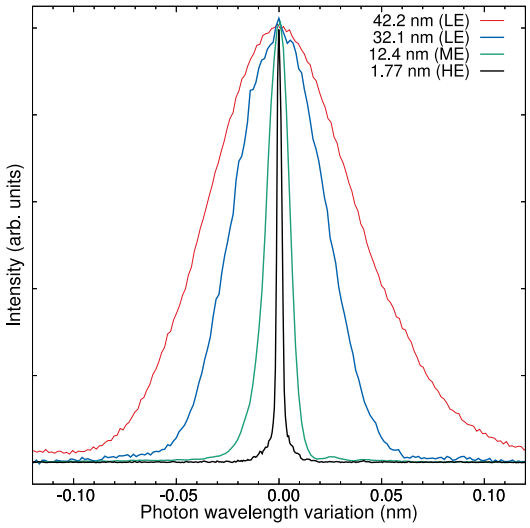

Fig. 6. Single-shot normalized spectra of FERMI as measured by WEST at four different FEL wavelengths. Spectra are plotted as a function of the variation from a central wavelength indicated in the legend.

Several FERMI single-shot spectra measured by WEST during different experimental runs are presented in Fig. 6. The figure reveals the impressive spectral properties of the FERMI FEL source inherited by the seed laser pulse. The spectral shape approximates that of a transform limited pulse in a wide photon energy range without using any monochromator. Estimated FEL FWHM bandwidths are 1.1 eV at 1.77 nm (700 eV), 0.1 eV at 12.4 nm (100 eV), 70 meV at 32.1 nm (39 eV), 60 meV at 42.2 nm (29 eV). The resolving power of WEST is appropriate to reproduce the FERMI spectrum in the entire spectral range of FERMI with an outstanding signal to noise ratio and almost negligible background.

Analysis of the photon energy mesh in the peaks of Fig. 6 confirms the theoretical trend of the WEST resolving power shown in Fig. 4 and provides indication that the experimental spectral resolution is compatible with the ray tracing simulations. Achieving the best resolving power requires the optimization of the distance r'. It was found during WEST operations that the depth of field of the grating is actually rather large, in the order of some centimeters. Therefore, the optimal focus of WEST can be set rather rapidly.

The photon detection sensitivity of WEST was found to be remarkable in the whole spectral range including the soft X-ray region. This feature permits to monitor on a single shot basis even the low intensity high harmonics emission of FERMI [45] extending significantly the range of accessible photon energies for various experimental techniques such as time resolved XAS.

4. Conclusions

We have described in detail the WEST spectrometer operating in transmission mode downstream of the TIMEX end station at the FERMI FEL. The design strategy of WEST, based on a slitless approach and single diffraction grating radically cuts fabrication and operation costs and can be easily exported to other soft X-ray FEL facilities interested in readily improving spectroscopies in transmission geometry. The basic parameters of WEST have been optimized for FERMI and the TIMEX beamline obtaining the best balance between efficiency and resolving power. The instrument maps the whole FERMI source spectral range including both the fundamental (EUV) and the highest harmonics emission (soft X-ray). Single-shot FEL spectra can be measured with excellent signal-to-noise ratio and negligible background. WEST is a versatile spectrometer that can be easily upgraded, for example changing the diffraction grating or the deviation angle, and adapted to different experimental soft X-ray FEL setups. A significant increase of the resolving power can be achieved either by operating the CCD of WEST in a more grazing incidence with respect to the FEL beam or positioning a suitable pinhole between the sample and the diffraction grating. Finally, WEST can be effectively employed in various emerging classes of FEL experiments encompassing, for example, time resolved absorption spectroscopy, stochastic spectroscopies, harmonics generation and stimulated emission.

Declaration of competing interest

The authors declare that they have no known competing financial interests or personal relationships that could have appeared to influence the work reported in this paper.

Data availability

Data will be made available on request.

Acknowledgments

We thank Michele Svandrlik and FERMI for funding the WEST project. The FERMI team is acknowledged for the assistance in assembling and operating the WEST spectrometer. Alessandro Baratti (Quantum Design s.r.l., Italy) is acknowledged for providing technical data on the Andor Ikon-M CCD camera.

Appendix A. Supplementary data

Supplementary material related to this article can be found online at https://doi.org/10.1016/j.nima.2023.168856.

References

[1] M. Yabashi, J.B. Hastings, M.S. Zolotorev, H. Mimura, H. Yumoto, S. Matsuyama, K. Yamauchi, T. Ishikawa, Single-shot spectrometry for X-ray free-electron lasers, Phys. Rev. Lett. 97 (2006) 084802.
[2] G. Brenner, S. Kapitzki, M. Kuhlmann, E. Ploenjes, T. Noll, F. Siewert, R. Treusch, K. Tiedtke, R. Reininger, M. Roper, M. Bowler, F. Quinn, J. Feldhaus, First results from the online variable line spacing grating spectrometer at flash, Nucl. Instrum. Methods Phys. Res. A 635 (1, Supplement) (2011) S99–S103.
[3] P. Karvinen, S. Rutishauser, A. Mozzanica, D. Greiffenberg, P.N. Juranić, A. Menzel, A. Lutman, J. Krzywinski, D.M. Fritz, H.T. Lemke, M. Cammarata, C. David, Single-shot analysis of hard X-ray laser radiation using a noninvasive grating spectrometer, Opt. Lett. 37 (2012) 5073–5075.
[4] D. Zhu, M. Cammarata, J.M. Feldkamp, D.M. Fritz, J.B. Hastings, S. Lee, H.T. Lemke, A. Robert, J.L. Turner, Y. Feng, A single-shot transmissive spectrometer for hard X-ray free electron lasers, Appl. Phys. Lett. 101 (3) (2012) 034103.
[5] M. Makita, P. Karvinen, D. Zhu, P.N. Juranic, J. Grünert, S. Cartier, J.H. Jungmann-Smith, H.T. Lemke, A. Mozzanica, S. Nelson, L. Patthey, M. Sikorski, S. Song, Y. Feng, C. David, High-resolution single-shot spectral monitoring of hard X-ray free-electron laser radiation, Optica 2 (10) (2015) 912–916.
[6] C. Svetina, D. Cocco, N. Mahne, L. Raimondi, E. Ferrari, M. Zangrando, PRESTO, the on-line photon energy spectrometer at FERMI: Design, features and commissioning results, J. Synchrotron Radiat. 23 (1) (2016) 35–42.
[7] M. Braune, G. Brenner, S. Dziarzhytski, P. Juranić, A. Sorokin, K. Tiedtke, A non-invasive online photoionization spectrometer for FLASH2, J. Synchrotron Radiat. 23 (1) (2016) 10–20.
[8] D. Rich, D. Zhu, J. Turner, D. Zhang, B. Hill, Y. Feng, The LCLS variable-energy hard X-ray single-shot spectrometer, J. Synchrotron Radiat. 23 (1) (2016) 3–9.
[9] J. Rehanek, M. Makita, P. Wiegand, P. Heimgartner, C. Pradervand, G. Seniutinas, U. Flechsig, V. Thominet, C. Schneider, A.R. Fernandez, C. David, L. Patthey, P. Juranic, The hard X-ray photon single-shot spectrometer of SwissFEL - initial characterization, J. Instrum. 12 (05) (2017) P05024.
[10] J. Rehanek, C.J. Milne, J. Szlachetko, J. Czapla-Masztafiak, J. Schneider, T. Huthwelker, C.N. Borca, R. Wetter, L. Patthey, P. Juranić, A compact and versatile tender X-ray single-shot spectrometer for online XFEL diagnostics, J. Synchrotron Radiat. 25 (1) (2018) 16–19.
[11] N. Kujala, W. Freund, J. Liu, A. Koch, T. Falk, M. Planas, F. Dietrich, J. Laksman, T. Maltezopoulos, J. Risch, F. Dall'Antonia, J. Grünert, Hard X-ray single-shot spectrometer at the European X-ray free-electron laser, Rev. Sci. Instrum. 91 (10) (2020) 103101.

[12] C. Arrell, V. Thominet, Y. Arbelo, U. Wagner, N. Gradwohl, E. Prat, L. Patthey, R. Follath, High resolution soft X-ray spectrometer for FEL characterisation and optimisation, in: Conference on Lasers and Electro-Optics, Optica Publishing Group, 2022, p. JTu3A.62.

[13] I. Inoue, E. Iwai, T. Hara, Y. Inubushi, K. Tono, M. Yabashi, Single-shot spectrometer using diamond microcrystals for X-ray free-electron laser pulses, J. Synchrotron Radiat. 29 (3) (2022) 862–865.

[14] S.H. Glenzer, R. Redmer, X-ray thomson scattering in high energy density plasmas, Rev. Modern Phys. 81 (2009) 1625–1663.

[15] L.B. Fletcher, U. Zastrau, E. Galtier, E.J. Gamboa, S. Goede, W. Schumaker, A. Ravasio, M. Gauthier, M.J. MacDonald, Z. Chen, E. Granados, H.J. Lee, A. Fry, J.B. Kim, C. Roedel, R. Mishra, A. Pelka, D. Kraus, B. Barbrel, T. Döppner, S.H. Glenzer, High resolution X-ray Thomson scattering measurements from cryogenic hydrogen jets using the linac coherent light source, Rev. Sci. Instrum. 87 (11) (2016) 11E524.

[16] A. Scherz, J. Schlappa, S. Parchenko, B. Van Kuiken, Y.Z, hRIXS instrument at EuXFEL, 2023, URL https://www.xfel.eu/facility/instruments/scs/index{_}eng.html.

[17] G. Dakovski, F. O'Dowd, K. Kunnus, C.G, Chemrixs/qRIXS instrument at LCLS, 2023, URL https://lcls.slac.stanford.edu/instruments/neh-2-2.

[18] C. Monney, L. Patthey, E. Razzoli, T. Schmitt, Static and time-resolved resonant inelastic X-ray scattering: Recent results and future prospects, X-ray Spectrometry (2022) 1–10.

[19] G. Ghiringhelli, A. Piazzalunga, C. Dallera, G. Trezzi, L. Braicovich, T. Schmitt, V.N. Strocov, R. Betemps, L. Patthey, X. Wang, M. Grioni, SAXES, a high resolution spectrometer for resonant X-ray emission in the 400-1600 eV energy range, Rev. Sci. Instrum. 77 (11) (2006) 113108.

[20] J. Dvorak, I. Jarrige, V. Bisogni, S. Coburn, W. Leonhardt, Towards 10 meV resolution: The design of an ultrahigh resolution soft X-ray RIXS spectrometer, Rev. Sci. Instrum. 87 (11) (2016) 115109.

[21] M. Beye, R.Y. Engel, J.O. Schunck, S. Dziarzhytski, G. Brenner, P.S. Miedema, Non-linear soft X-ray methods on solids with musix - the multi-dimensional spectroscopy and inelastic X-ray scattering endstation, J. Phys. Condensed Matter 31 (1) (2019) 014003.

[22] Y.-D. Chuang, X. Feng, A. Cruz, K. Hanzel, A. Brown, A. Spucces, A. Frano, W.-S. Lee, J. Kim, Y.-J. Chen, B. Smith, J.S. Pepper, Y.-C. Shao, S.-W. Huang, L.A. Wray, E. Gullikson, Z.-X. Shen, T.P. Devereaux, A. Tremsin, W. Yang, J. Guo, R. Duarte, Z. Hussain, Momentum-resolved resonant inelastic soft X-ray scattering (qRIXS) endstation at the ALS, J. Electron Spectrosc. Relat. Phenom. 257 (2022) 146897.

[23] R. Alonso-Mori, J. Kern, R.J. Gildea, D. Sokaras, T.-C. Weng, B. Lassalle-Kaiser, R. Tran, J. Hattne, H. Laksmono, J. Hellmich, C. Glöckner, N. Echols, R.G. Sierra, D.W. Schafer, J. Sellberg, C. Kenney, R. Herbst, J. Pines, P. Hart, S. Herrmann, R.W. Grosse-Kunstleve, M.J. Latimer, A.R. Fry, M.M. Messerschmidt, A. Miahnahri, M.M. Seibert, P.H. Zwart, W.E. White, P.D. Adams, M.J. Bogan, S. Boutet, G.J. Williams, A. Zouni, J. Messinger, P. Glatzel, N.K. Sauter, V.K. Yachandra, J. Yano, U. Bergmann, Energy-dispersive X-ray emission spectroscopy using an X-ray free-electron laser in a shot-by-shot mode, Proc. Natl. Acad. Sci. 109 (47) (2012) 19103–19107.

[24] N. Rohringer, D. Ryan, R.A. London, M. Purvis, F. Albert, J. Dunn, J.D. Bozek, C. Bostedt, A. Graf, R. Hill, S.P. Hau-Riege, J.J. Rocca, Atomic inner-shell X-ray laser at 1.46 nanometres pumped by an X-ray free-electron laser, Nature 481 (7382) (2012) 488–491.

[25] S. Yamamoto, T. Omi, H. Akai, Y. Kubota, Y. Takahashi, Y. Suzuki, Y. Hirata, K. Yamamoto, R. Yukawa, K. Horiba, H. Yumoto, T. Koyama, H. Ohashi, S. Owada, K. Tono, M. Yabashi, E. Shigemasa, S. Yamamoto, M. Kotsugi, H. Wadati, H. Kumigashira, T. Arima, S. Shin, I. Matsuda, Element selectivity in second-harmonic generation of $gafeo_3$ by a soft-X-ray free-electron laser, Phys. Rev. Lett. 120 (2018) 223902.

[26] T. Helk, E. Berger, S. Jamnuch, L. Hoffmann, A. Kabacinski, J. Gautier, F. Tissandier, J.-P. Goddet, H.-T. Chang, J. Oh, C.D. Pemmaraju, T.A. Pascal, S. Sebban, C. Spielmann, M. Zuerch, Table-top extreme ultraviolet second harmonic generation, Sci. Adv. 7 (21) (2021) eabe2265.

[27] R.K. Lam, S.L. Raj, T.A. Pascal, C.D. Pemmaraju, L. Foglia, A. Simoncig, N. Fabris, P. Miotti, C.J. Hull, A.M. Rizzuto, J.W. Smith, R. Mincigrucci, C. Masciovecchio, A. Gessini, E. Allaria, G. De Ninno, B. Diviacco, E. Roussel, S. Spampinati, G. Penco, S. Di Mitri, M. Trovò, M. Danailov, S.T. Christensen, D. Sokaras, T.-C. Weng, M. Coreno, L. Poletto, W.S. Drisdell, D. Prendergast, L. Giannessi, E. Principi, D. Nordlund, R.J. Saykally, C.P. Schwartz, Soft X-ray second harmonic generation as an interfacial probe, Phys. Rev. Lett. 120 (2018) 023901.

[28] C.P. Schwartz, S.L. Raj, S. Jamnuch, C.J. Hull, P. Miotti, R.K. Lam, D. Nordlund, C.B. Uzundal, C. Das Pemmaraju, R. Mincigrucci, L. Foglia, A. Simoncig, M. Coreno, C. Masciovecchio, L. Giannessi, L. Poletto, E. Principi, M. Zuerch, T.A. Pascal, W.S. Drisdell, R.J. Saykally, Angstrom-resolved interfacial structure in buried organic–inorganic junctions, Phys. Rev. Lett. 127 (2021) 096801.

[29] C. Ferrante, E. Principi, A. Marini, G. Batignani, G. Fumero, A. Virga, L. Foglia, R. Mincigrucci, A. Simoncig, C. Spezzani, C. Masciovecchio, T. Scopigno, Non-linear self-driven spectral tuning of extreme ultraviolet femtosecond pulses in monoatomic materials, Light: Sci. Appl. 10 (2021) 92.

[30] A. Levy, F. Dorchies, C. Fourment, M. Harmand, S. Hulin, J.J. Santos, D. Descamps, S. Petit, R. Bouillaud, Double conical crystal X-ray spectrometer for high resolution ultrafast X-ray absorption near-edge spectroscopy of Al?K edge, Rev. Sci. Instrum. 81 (6) (2010) 063107.

[31] B.I. Cho, K. Engelhorn, A.A. Correa, T. Ogitsu, C.P. Weber, H.J. Lee, J. Feng, P.A. Ni, Y. Ping, A.J. Nelson, D. Prendergast, R.W. Lee, R.W. Falcone, P.A. Heimann, Electronic structure of warm dense copper studied by ultrafast X-ray absorption spectroscopy, Phys. Rev. Lett. 106 (2011) 167601.

[32] G. Brenner, S. Dziarzhytski, P.S. Miedema, B. Rösner, C. David, M. Beye, Normalized single-shot X-ray absorption spectroscopy at a free-electron laser, Opt. Lett. 44 (9) (2019) 2157–2160.

[33] E. Principi, S. Krylow, M.E. Garcia, A. Simoncig, L. Foglia, R. Mincigrucci, G. Kurdi, A. Gessini, F. Bencivenga, A. Giglia, S. Nannarone, C. Masciovecchio, Atomic and electronic structure of solid-density liquid carbon, Phys. Rev. Lett. 125 (2020) 155703.

[34] E. Principi, E. Giangrisostomi, R. Mincigrucci, M. Beye, G. Kurdi, R. Cucini, A. Gessini, F. Bencivenga, C. Masciovecchio, Extreme ultraviolet probing of nonequilibrium dynamics in high energy density germanium, Phys. Rev. B 97 (2018) 174107.

[35] Y. Kayser, C. Milne, P. Juranić, L. Sala, J. Czapla-Masztafiak, R. Follath, M. Kavčič, G. Knopp, J. Rehanek, W. Bł achucki, M.G. Delcey, M. Lundberg, K. Tyrala, D. Zhu, R. Alonso-Mori, R. Abela, J. Sá, J. Szlachetko, Core-level nonlinear spectroscopy triggered by stochastic X-ray pulses, Nature Commun. 10 (2019) 4761.

[36] D. De Angelis, E. Principi, F. Bencivenga, D. Fausti, L. Foglia, Y. Klein, M. Manfredda, R. Mincigrucci, A. Montanaro, E. Pedersoli, J.S. Pelli Cresi, G. Perosa, K.C. Prince, E. Razzoli, S. Shwartz, A. Simoncig, S. Spampinati, C. Svetina, J. Szlachetko, A. Tripathi, I.A. Vartanyants, M. Zangrando, F. Capotondi, Free electron laser stochastic spectroscopy revealing silicon bond softening dynamics, Phys. Rev. B 107 (2023) 214305.

[37] R. Mincigrucci, J.R. Rouxel, B. Rossi, E. Principi, C. Bottari, S. Catalini, J.S. Pelli-Cresi, D. Fainozzi, L. Foglia, A. Simoncig, A. Matruglio, G. Kurdi, F. Capotondi, E. Pedersoli, A. Perucchi, F. Piccirilli, A. Gessini, M. Giarola, G. Mariotto, M. Oppermann, S. Mukamel, F. Bencivenga, M. Chergui, C. Masciovecchio, Element- and enantiomer-selective visualization of molecular motion in real-time, Nature Commun. 14 (2023) 386.

[38] D. Keefer, T. Schnappinger, R. de Vivie-Riedle, S. Mukamel, Visualizing conical intersection passages via vibronic coherence maps generated by stimulated ultrafast X-ray Raman signals, Proc. Natl. Acad. Sci. 117 (39) (2020) 24069–24075.

[39] E. Allaria, R. Appio, L. Badano, W.A. Barletta, S. Bassanese, M. Zangrando, Highly coherent and stable pulses from the FERMI seeded free-electron laser in the extreme ultraviolet, Nat. Phot. 6 (2012) 699–704.

[40] E. Allaria, D. Castronovo, P. Cinquegrana, P. Craievich, M. Dal Forno, M.B. Danailov, G. D'Auria, A. Demidovich, G. De Ninno, S. Di Mitri, B. Diviacco, W.M. Fawley, M. Ferianis, E. Ferrari, L. Froehlich, G. Gaio, D. Gauthier, L. Giannessi, R. Ivanov, B. Mahieu, N. Mahne, I. Nikolov, F. Parmigiani, G. Penco, L. Raimondi, C. Scafuri, C. Serpico, P. Sigalotti, S. Spampinati, C. Spezzani, M. Svandrlik, C. Svetina, M. Trovo, M. Veronese, D. Zangrando, M. Zangrando, Two-stage seeded soft-X-ray free-electron laser, Nature Photonics 7 (11) (2013) 913–918.

[41] L. Giannessi, C. Masciovecchio, FERMI: Present and future challenges, Appl. Sci. 7 (6) (2017) 640.

[42] C. Masciovecchio, A. Battistoni, E. Giangrisostomi, F. Bencivenga, E. Principi, R. Mincigrucci, R. Cucini, A. Gessini, F. D'Amico, R. Borghes, M. Prica, V. Chenda, M. Scarcia, G. Gaio, G. Kurdi, A. Demidovich, M.B. Danailov, A. Di Cicco, A. Filipponi, R. Gunnella, K. Hatada, N. Mahne, L. Raimondi, C. Svetina, R. Godnig, A. Abrami, M. Zangrando, EIS: The scattering beamline at FERMI, J. Synch. Rad. 22 (3) (2015) 553–564.

[43] T. Namioka, Theory of the concave grating, I, J. Opt. Soc. Am. 49 (5) (1959) 446–460.

[44] T. Namioka, T. Haga, H. Kinoshita, What can we do for soft X-ray optics by ray tracing, in: JSPE Proceedings on Soft X-ray Optics, Japan Society for Precision Engineering, 1997, pp. 185–198.

[45] G. Penco, G. Perosa, E. Allaria, L. Badano, F. Bencivenga, A. Brynes, C. Callegari, F. Capotondi, A. Caretta, P. Cinquegrana, S. Dal Zilio, M.B. Danailov, D. De Angelis, A. Demidovich, S. Di Mitri, L. Foglia, G. Gaio, A. Gessini, L. Giannessi, G. Kurdi, M. Manfredda, M. Malvestuto, C. Masciovecchio, R. Mincigrucci, I. Nikolov, E. Pedersoli, S. Pelli Cresi, E. Principi, P. Rebernik, A. Simoncig, S. Spampinati, C. Spezzani, F. Sottocorona, M. Trovó, M. Zangrando, V. Chardonnet, M. Hennes, J. Lüning, B. Vodungbo, P. Bougiatioti, C. David, B. Roesner, M. Sacchi, E. Roussel, E. Jal, G. De Ninno, Nonlinear harmonics of a seeded free-electron laser as a coherent and ultrafast probe to investigate matter at the water window and beyond, Phys. Rev. A 105 (2022) 053524.

[46] M. Neviere, Diffraction of light by gratings studied with the differential method, in: Proc. SPIE 0240, 1981.

[47] F. Schäfers, M. Krumrey, Technical Report Tb 201, BESSY, Berlin, Germany, 1996, pp. 1–17.

[48] L. Rebuffi, M. Sánchez del Río, ShadowOui: A new visual environment for X-ray optics and synchrotron beamline simulations, J. Synchrotron Radiat. 23 (6) (2016) 1357–1367.

[49] M. Zangrando, A. Abrami, D. Bacescu, I. Cudin, C. Fava, F. Frassetto, A. Galimberti, R. Godnig, D. Giuressi, L. Poletto, L. Rumiz, R. Sergo, C. Svetina, D. Cocco, The photon analysis, delivery, and reduction system at the FERMI@Elettra free electron laser user facility, Rev. Sci. Instrum. 80 (11) (2009) 113110.

[50] K. Lieutenant, T. Hofmann, C. Zendler, C. Schulz, E.F. Aziz, K. Habicht, Numerical optimization of a RIXS spectrometer using raytracing simulations, J. Phys. Conf. Ser. 738 (1) (2016) 012104.

[51] 2020. https://andor.oxinst.com/assets/uploads/products/andor/documents/andor-ikon-l-and-m-so-specifications.pdf.